Polarization-dependent electrocaloric and pyroelectric effects in ferroelectric $BaTiO_3$ thin films

J. W. Adkins[1,2,5*], I. Fina[3], F. Sánchez[3], S. R. Bakaul[2*], and J. T. Abiade[1,4,5]

[1]*Department of Civil, Materials and Environmental Engineering, University of Illinois Chicago, Chicago, IL 60607, USA*
[2]*Materials Science Division, Argonne National Laboratory, Lemont, IL 60439, USA*
[3]*Institut de Ciència de Materials de Barcelona (ICMAB-CSIC), Campus UAB, Bellaterra 08193, Barcelona, Spain*
[4]*Department of Mechanical and Industrial Engineering, University of Illinois Chicago, Chicago, IL 60607, USA*
[5]*Laboratory for Oxide Research and Education, 842 W. Taylor Street, Chicago, IL 60607, USA*

*Corresponding authors, jadkin3@uic.edu, saidur.bakaul@gmail.com

Abstract:

Herein we examine the influence of controllable polarization reversal and built-in electric fields on pyroelectric and electrocaloric effects in a $BaTiO_3$ thin film using a modified indirect method. We find that the magnitude of the sample's change in polarization with temperature is sensitive to the degree of polarization reversal. The pyroelectric response is small at low fractions of switched polarization and grows larger by several factors as larger fractions of polarization are reversed. This polarization reversal-sensitive pyroelectric behavior is the result of an internal built-in field, which has the effect of destabilizing low fractions of switched polarization and producing a diminished pyroelectric effect. Greater fractions of switched polarization are more stable against backswitching and permit a larger pyroelectric response. Our findings highlight a characterization method for polarization-dependent pyroelectric effects in ferroelectric thin films where built-in field effects are also present.

Pyroelectricity occurs in all ferroelectrics and manifests as a temperature-induced change in electric polarization[1,2]. Pyroelectric phenomena, as well as closely related electrocaloric phenomena, are of notable technological relevance, as can be seen by persistent scientific interest in their biomedical[3,4], sensor[5–8], and energy harvesting/conversion[9–12] applications. Pyroelectricity in ferroelectric materials possesses several contributions. The primary effect, which is tied to intrinsic changes in polarization with temperature and extrinsic changes in domain configuration with temperature, is described by Eq. 1.[13]:

$$\pi = \varphi_C \frac{d\langle P\rangle}{dT} + \langle P\rangle \frac{d\varphi_C}{dT} \quad (1)$$

Primary effects dominate in bulk ferroelectrics. When examined as thin films fabricated on rigid substrates, ferroelectrics also exhibit secondary and tertiary contributions to pyroelectricity to due thermal mismatch-induced piezoelectric effects and electric field-driven phenomena, respectively.

Numerous efforts to understand and control these contributions within the context of the operational temperature range and total magnitude of pyroelectric effects in ferroelectrics for wide-scale applications are ongoing; composition-[14,15],strain-[16,17], and field-driven[18–20] investigations are ubiquitous.

Field-driven control of pyroelectricity in bulk[8,21–23] and thin film[24–26] ferroelectrics benefits from requiring 'simply' the examination of material response to highly programmable stimuli in the form of biasing, but includes further complications due to dielectric and leakage contributions. Nevertheless, investigations related to the influence of applied electric fields on pyroelectric effects have remained an active area of inquiry and have theoretically[13,27] and experimentally[28,29] demonstrated an additional avenue of control in ferroelectric materials. Within the context of field-dependent studies of ferroelectric thin films, the impact of built-in fields cannot be understated. Built-in fields generally manifest as a shift in polarization-electric field (P-E) hysteresis loops[30]. Several factors can induce such fields, such as compositional gradients[31], substrate clamping[32], and uneven distributions of defects[30,33]. Asymmetric electrodes may also generate built-in fields, through differences in work functions and interfacial conditions[34]. These fields can and will influence pyroelectric and electrocaloric effects[35–37].

When considering the various contributions to pyroelectric and electrocaloric effects, several methods offer varying degrees of effectiveness and accuracy. These methodologies are often grouped into two categories[38]: (i) direct methods, which directly measure pyrocurrents or temperature changes due to controlled temperature fluctuations or field pulses, respectively[39–41], and (ii) indirect methods, which collect temperature-dependent hysteresis loops and use Maxwell relations assuming thermodynamic reversibility to approximate pyroelectric and electrocaloric effects[42,43]. Direct methods can be quite accurate with respect to primary effects due to the absence of biasing during measurements but require specific device configurations and specialized equipment that limit accessibility. Indirect methods sacrifice sensitivity to primary pyroelectric contributions for greater accessibility, rapid collection, and preliminary predictions for interesting electrocaloric phenomena[19,44]. Considering these facts, it is often of benefit to compromise by way of modified or pseudo-methods[45]. Modified indirect methods that utilize unipolar pulses, for example, can be used to emulate the reversible conditions required for accurate use of Maxwell relations[46]. To study pyroelectric and electrocaloric effects in a $BaTiO_3$ thin film, we developed a modified pseudo-indirect method, which employs electric field pulse protocols to selectively reverse different extents of polarization. Using it, we investigated the influence of polarization reversal on the pyroelectric properties of an internally biased $BaTiO_3$ thin film.

100-nm thick ferroelectric $BaTiO_3$ (BTO) and 25-nm thick $La_{2/3}Sr_{1/3}MnO_3$ (LSMO) bottom electrodes films were grown on single crystal (001)-oriented $SrTiO_3$ (STO) substrates via pulsed laser deposition (PLD) using a 248-nm KrF excimer laser. BTO was deposited at substrate temperature of 675 °C and oxygen pressure of 0.02 mbar, optimal for epitaxial growth on LSMO electrodes. Laser frequency was 5 Hz and the growth rate 0.50 Å/pulse. Additional details can be found elsewhere[47]. 40 µm x 40 µm 100-nm thick platinum top electrodes were lithographically deposited onto photoresisted BTO films via electron beam evaporation. Ferroelectric measurements were conducted using a Radiant Technologies Precision Premier II ferroelectric

tester and low-temperature high-vacuum conditions were achieved with the use of a Lakeshore Cryogenic Probe Station. Full hysteresis loops in the range of 100 K to 235 K were collected with a maximum applied bias of 25.5V (255 MVm^{-1}) and 10 kHz frequency; P-E hysteresis loops between 40 K and 100 K were collected with a maximum applied bias of 40 V (400 MVm^{-1}) and 10 kHz frequency. To calibrate reversable polarization states in the BTO films at various temperatures and approximate the corresponding pyroelectric behavior due to polarization reversal, a three-step erase-write-read collection sequence of monopolar hysteresis loops was programmed (Supplementary Information Sec. S1). All monopolar pulses are delivered at a 20 kHz frequency. The first monopolar pulse train (Fig. S1A) is used to pre-pole the ferroelectric with a large negative AC bias of 25.5V. The following positive monopolar pulse (Fig. S1B) varies in magnitude from 0V to 25.5V and partially switches BTO. The final monopolar pulse (Fig. S1C) reads the domain-configured film's polarization with a fixed magnitude of 25.5V. This three-pulse sequence was applied between 100 K to 235 K, in 15 K increments. Minor loops illustrating various extents of written polarization reversal are included in Supplementary Information Sec. S2.To observe polarization-dependent pyroelectric effects more directly[46], an additional four-step erase-write-read-read collection sequence of monopolar hysteresis loops was programmed (Supplementary Information Sec. S3). This pulse sequence is collected at 100 K and 40 K, with the difference in read polarization used to approximate pyroelectric effects. A time delay of about 30 minutes is required to adjust the temperature of the sample from 100 K to 40 K. Electromechanical confirmation of ferroelectricity in the BTO thin films was acquired using a dual-AC resonance tracking switching spectroscopy (DART-SS) technique of piezoresponse force microscopy[48], with an Asylum Research MPF-3D atomic force microscope. DART-SS measurements were conducted on top of the Pt electrodes with a 7.5 V DC max tip bias, 300 mV AC drive bias, 1 Hz pulse frequency, and 5 ms pulse period. To avoid contributions from purely electrostatic piezoresponse signals, the piezoresponse data reported here were only collected from the periods in between tip bias applications[49].

Figure 1 presents room-temperature structural, electrical, and electromechanical characterization of the BTO thin film. The θ-2θ x-ray diffraction pattern in Fig. 1A shows intense peaks corresponding to STO (00l) substrate reflections. The corresponding LSMO (00l) and BTO (00l) reflections are at the right and the left of the substrate peaks, respectively. The BTO (002) reflection is a double peak. The low and high intensity BTO (002) peaks are at $2\theta = 41.85^{\circ}$ (c = 0.4317 nm) and $2\theta = 43.61^{\circ}$ (c = 0.4152 nm). The out-of-plane lattice parameter corresponding to both peaks is larger than the c-parameter of bulk BTO (c=0.4038 nm), indicating that the BTO film is tetragonal, c-oriented and both highly and inhomogeneously strained. The lattice mismatch between BTO and STO is 2.2%, and the compressive epitaxial strain of thick BTO films relaxes above a deposition parameter-dependent critical thickness[50]. The large out-of-plane strain corresponding to the peaks, 2.8% and 6.9%, is due to elastic deformation and also to point defects usual in BTO films deposited by PLD[47,51]. In the presence of such a large tensile strain, the material under study is not expected to exhibit phase transformations capable of influencing pyroelectric phenomena across the temperature window examined[52,53]. Both P-E (Fig. 1B) and PFM (Fig. 1C) hysteresis confirm the presence of ferroelectricity in BTO, with the addition of a noticeable imprint effect manifesting as a shift in positive and negative coercive fields to more positive values by

about 1.6 V (16 MVm^{-1}). This suggests that the ferroelectric thin film has a preferential negative polarization potentially induced by asymmetry in the top (Pt) and bottom (LSMO) electrodes. Liu and coworkers reported a similar effect in Pt/BTO/LSMO MIM structures, defining the imprint field E_{imp} as $(E_{c+} + E_c)/2$. The value they report for the magnitude of E_{imp} is about 12 MVm^{-1} at a measurement frequency of 15 kHz, which is close to the value we report here[54].

Temperature-dependent monopolar P-E hysteresis data are provided in Figure 2. Fig. 2A illustrates the minor loops acquired from the 2nd write pulse of the three-pulse sequence. At the maximum applied field, the system's switchable maximum and remanent polarization, as well as coercive field, decrease with temperature; at 100 K, the maximum and remanent polarization are 26.5 $\mu C/cm^2$ and 15.1 $\mu C/cm^2$, respectively, and decrease to 22.7 $\mu C/cm^2$ and 6.3 $\mu C/cm^2$ at 235 K. The large discrepancies between the maximum and remanent polarization are indicative of pronounced leakage and backswitching effects[55], which are further exacerbated by the horizontal shift in monopolar hysteresis loop due to imprint. To indirectly approximate the extent of polarization in the ferroelectric, the evolution of the double remanent polarization ($2P_{r,write} = P^{+}_{r,write} - P^{-}_{r,write}$) collected with the three-pulse sequence's variable-magnitude write pulse is plotted against the applied electric field (Fig. 2B) across the measurement temperature range. We consider the ferroelectric saturated when the double remanent polarization begins to increase linearly with increasing field, which indicates that no further ferroelectric switching is occurring. After the saturation field is identified for each temperature, we normalize the $2P_{r,write}$ values against the value of the polarization at E_{sat} to present the fraction of switched polarization as the applied electric field increases, an example of which is provided in Fig. 2C for T = 160 K. Calibrated E_{sat} and E_C data for all other measurement temperatures are included in Fig. 2D. Predictably, we observe a linear increase in coercivity as temperature decreases[56]. Other fractions of switched polarization are controlled by considering the 2nd pulse magnitude and are included for all measurement temperatures in Supplementary Information Sec. S4.

After calibrating switched polarization for BTO at a given 2nd pulse magnitude and temperature, we analyzed the influence of switched polarization on the pyroelectric behavior. Fig. 3A presents the evolution of the $2P_{r,write}$ with temperature at different fractions of switched polarization. We find that at low fractions of switched polarization, the temperature dependence of polarization is quite weak – this is reflected in the miniscule value of the pyroelectric effect (-137 $\mu Cm^{-2}K^{-1}$) shown in Fig. 3B for a 10% switched polarization configuration. This pyroelectric effect *p* is approximated via Eq. 2:

$$p = \frac{\Delta 2P_r}{\Delta T} = \frac{2P_{r(lo)} - 2P_{r(hi)}}{T_{lo} - T_{hi}} \quad (2)$$

where T_{hi} = 235 K, T_{lo} = 100 K, $2P_{r(hi)}$ is the written double remanent polarization at 235 K, and $2P_{r\ (lo)}$ is the written double remanent polarization at 100 K. Comparatively, switching greater fractions of polarization at each temperature induces a larger apparent pyroelectric effect, with a much larger effect (~ -1270 $\mu Cm^{-2}K^{-1}$) for a 90% switched polarization configuration. Identical behavior is observed for the $2P_{r,read}$ values shown in Fig. 3C. Furthermore, no discontinuities in the polarization vs. temperature data are observed, which supports our

preliminary predictions of phase stability. Though the relationship between switched polarization and the pyroelectric effect under study appears to superficially invert when considering the read polarization of the third pulse, the actual behavior shown in Fig. 3D is consistent when considering that both pulses can induce polarization switching. As such, the $2P_{r,read}$ values for the 10% switched polarization condition includes switching contributions from the rest of the unswitched polarization and should be compared to the equivalent 90% switched polarization condition for the $2P_{r,write}$ of the write pulse. Nevertheless, calculated pyroelectric effects from $2P_{r,read}$ values are, on average, about 25% higher than those determined from equivalent written $2P_{r,write}$ values. This is most evident when comparing the pyroelectric effect under 50% switched polarization conditions for the read and write pulses, which are approximately -890 $\mu Cm^{-2}K^{-1}$ and -700 $\mu Cm^{-2}K^{-1}$, respectively. Though we cannot currently identify the exact origin of this increase, we speculate that a combination of hysteretic leakage and dielectric effects may be the cause.

To further examine the polarization- and built-in field-dependent pyroelectric behavior in the BTO thin film, we used an alternative four-pulse measurement protocol conducted between 100 K and 40 K. Across this temperature regime, leakage effects are minimized and contributions to pyroelectric effects from phase transformations are avoided. A variable-temperature analysis of device imprint was also conducted at select temperatures between 100 K and 40 K to confirm that the magnitude of the built-in field did not change substantially with temperature (Supplementary Information Sec. S5). Pyroelectric effects are approximated via Eq. 3:

$$p = \frac{\Delta 2P_r}{\Delta T} = \frac{(2P_{r,2} - 2P_{r,1})_{lo} - (2P_{r,2} - 2P_{r,1})_{hi}}{T_{lo} - T_{hi}} \quad (3)$$

Here, $2P_{r,1}$ and $2P_{r,2}$ are the double remanent polarization of first and second read pulses, across a temperature range $\Delta T = 60$ K. Read pulses are applied both at 100 K (Fig. 4A) and 40 K (Fig. 4B) after polarization is written at 100 K, with the latter achieved by cooling the sample by 60 K over 30 minutes before measurement. The pyroelectric effect (Fig. 4C) remains small at low fractions of switched polarization (~ -20 ± 80 $\mu Cm^{-2}K^{-1}$) and grows by a factor of 15 to -270 ± 90 $\mu Cm^{-2}K^{-1}$ as the fraction of switched polarization approaches 100%. That this observation is consistent with the three-pulse protocol's results lends support to the pyroelectric effect's polarization dependence as occurring irrespective of phase transformations and leakage effects. The delay between writing variable fractions of polarization at 100 K and reading the polarization at 40 K may also contribute to the lower size of the pyroelectric effects reported here as compared to the three-pulse protocol, whose rapid measurement suppresses relaxation effects. Regardless, the maximum value of the pyroelectric effect reported here is in good agreement with values between -200 and -400 $\mu Cm^{-2}K^{-1}$ reported elsewhere in the literature[57–59]. Both three-pulse and four-pulse protocols demonstrate that the degree of polarization reversal greatly affects the pyroelectric behavior of BTO.

Considering the miniscule size of the pyroelectric behavior under mostly-unswitched conditions, which run counter-intuitive to general trends in ferroelectric polarization with temperature, we argue that the sensitivity is the result of the sample's built-in field. The destabilizing effects of a built-in field are well documented for perovskites[60–62], and in the case of

$BaTiO_3$ thin films, these effects should be even more pronounced[63]. When further considering that the built-in field in this sample is quite large (~16 MVm^{-1}), it becomes more apparent that the polarization-dependent pyroelectric effect calculated here are greatly influence by polarization destabilization. This is evidenced by the magnitude of two variables associated with our calculations: $2P_{r,1}$ and $2P_{r,2}$. The difference between $2P_{r,1}$ values collected at 100 K and 40 K is dependent upon previously written polarization – greater than ~0.3 μCcm^{-2} before 50% polarization reversal and less than ~0.3 μCcm^{-2} beyond 50% polarization reversal. On the other hand, the values of $2P_{r,2}$ consistently vary by about 2 $\mu C\ cm^{-2}$ when measured at the same two temperatures. These observations are consistent with a built-in field that backswitches polarization after every read pulse. When the behaviors of these two values are considered within the context of Eq. 4, a generality appears:

$$p = \frac{\Delta 2P_r}{\Delta T} = \frac{\left(2P_{r,2(lo)} - 2P_{r,2(hi)}\right)}{T_{lo} - T_{hi}} + \frac{\left(2P_{r,1(hi)} - 2P_{r,1(lo)}\right)}{T_{lo} - T_{hi}} \quad (4)$$

Under conditions where the first term is relatively large and positive (i. e. when low fractions of polarization are reversed), the second term, which is always negative, results in a miniscule pyroelectric effect. However, when the first term is relatively small (when high fractions of polarization are reversed), a larger negative pyroelectric effect is observed. Briefly, we consider the implications of this observation for influencing electrocaloric temperature changes. The anticipated adiabatic temperature change induced by an applied field is given by[38]

$$\Delta T = -\frac{T}{\rho C} p \Delta E \quad (5)$$

where T is the temperature, p is the pyroelectric coefficient, ρ is the density (~6020 kgm^{-3} for $BaTiO_3$), C the heat capacity (~ 680 $Jkg^{-1}K^{-1}$)[64], and ΔE the difference between the minimum and maximum fields applied during electrocaloric cycling. If the initial domain configuration in the ferroelectric device under study is controlled prior to field cycling, such that the magnitude of p is controlled as we have demonstrated, it is possible to amplify resulting temperature change ΔT. We illustrate this amplification in Fig. 4D, where we have estimated the projected ΔT for the magnitude of the pyroelectric effect at the fractions of switched polarization examined, assuming T = 293 K and ΔE = 0.5 MVm^{-1}. The magnitude of this effect – at most several millikelvin - is small compared to both cooling that directly utilizes order-disorder transitions in $BaTiO_3$ [65], as well as our own indirect estimates of the electrocaloric effect in $BaTiO_3$ using saturated minor loops (Supplementary Information Sec. S6). However, it nevertheless represents the influence of polarization instabilities due to a built-in field on pyroelectric and electrocaloric effects in ferroelectric thin films.

In summary, we have demonstrated a modified indirect method to examine polarization-dependent pyroelectric effects in a $BaTiO_3$ thin film. The method involves controlling the degree of polarization reversal using a multi-pulse protocol to indirectly compute polarization-dependent pyroelectric phenomena at varying temperatures. We have observed polarization-din tandem with utilizing the destabilizing effects of a built-in electric field. This thermally stable built-in field,

likely induced by asymmetry in the ferroelectric device's electrode configuration, has the effect of minimizing pyroelectric effects in BTO when small fractions of switched polarization are used to evaluate pyroelectric phenomena and can be overcome by increasing the extent of polarization reversal. Our findings highlight a characterization method for polarization-dependent pyroelectric effects in ferroelectric thin films where built-in field effects are also present.

Supplementary Material

See supplementary material for information regarding the multi-pulse measurement protocols, normalization of written polarization against the saturation polarization at all measurement temperatures, temperature-dependent imprint behavior, and additional electrocaloric temperature lift estimates.

Acknowledgements

J. T. Abiade acknowledges financial support from the U. S. National Science Foundation under Grant No. NSFDMR-1508220. Financial support from the Spanish Ministry of Science and Innovation (10.13039/501100011033), through the Severo Ochoa FUNFUTURE (project CEX2019-000917-S funded by MCIN/AEI), project TED2021-130453B-C21 funded by MCIN/AEI and European Union NextGenerationEU/PRTR, and projects PID2020-112548RB-I00 and PID2019-107727RB-I00 funded by MCIN/AEI are acknowledged. J. W. Adkins acknowledges the University of Illinois Chicago's Pipeline to an Inclusive Faculty (PIF) Program. The work (Electronic measurements and part of manuscript preparation) at Argonne National Laboratory were supported by the U.S. Department of Energy, Office of Science, Basic Energy Sciences, Materials Sciences and Engineering Division. Lithographic patterning was conducted using equipment provided by the University of Illinois Chicago's Nanotechnology Core Facility.

Data Availability Statement

The data that support the findings of this study are available from the corresponding author upon reasonable request.

References

[1] M.E. Lines and A.M. Glass, *Principles and Applications of Ferroelectrics and Related Materials* (Oxford University Press, Oxford, 1977).

[2] M. Dawber, K.M. Rabe, and J.F. Scott, Rev. Mod. Phys. **77**, 1083 (2005).

[3] S. Kumar, M. Sharma, T. Frömling, and R. Vaish, J. Ind. Eng. Chem. (2021).

[4] W. Wang, J. Li, H. Liu, and S. Ge, Adv. Sci. **8**, 1 (2021).

[5] R.W. Whatmore, P.C. Osbond, and N.M. Shorrocks, Ferroelectrics **76**, 351 (1987).

[6] W.N. Lawless, J. Opt. Soc. Am. **62**, 1449 (1972).

[7] J.H. Yoo, W. Gao, and K.H. Yoon, J. Mater. Sci. **34**, 5361 (1999).

[8] B.M. Kulwicki, A. Amin, H.R. Beratan, and C.M. Hanson, ISAF 1992 - Proc. 8th IEEE Int. Symp. Appl. Ferroelectr. 1 (1992).

[9] M. Hoffmann, U. Schroeder, C. Künneth, A. Kersch, S. Starschich, U. Böttger, and T. Mikolajick, Nano Energy **18**, 154 (2015).

[10] S. Pandya, J. Wilbur, J. Kim, R. Gao, A. Dasgupta, C. Dames, and L.W. Martin, Nat. Mater. **17**, 432 (2018).

[11] C.R. Bowen, J. Taylor, E. Leboulbar, D. Zabek, A. Chauhan, and R. Vaish, Energy Environ. Sci. **7**, 3836 (2014).

[12] G. Sebald, E. Lefeuvre, and D. Guyomar, IEEE Trans. Ultrason. Ferroelectr. Freq. Control **55**, 538 (2008).

[13] J. Karthik and L.W. Martin, Phys. Rev. B - Condens. Matter Mater. Phys. **84**, 1 (2011).

[14] S.W. Smith, A.R. Kitahara, M.A. Rodriguez, M.D. Henry, M.T. Brumbach, and J.F. Ihlefeld, Appl. Phys. Lett. **110**, 0 (2017).

[15] P. Qiao, Y. Zhang, X. Chen, M. Zhou, G. Wang, and X. Dong, Ceram. Int. **45**, 7114 (2019).

[16] X. Zhang, J.B. Wang, B. Li, X.L. Zhong, X.J. Lou, and Y.C. Zhou, J. Appl. Phys. **109**, 1 (2011).

[17] V.B. Shirokov, A.G. Razumnaya, and Y.I. Yuzyuk, J. Phys. Condens. Matter **29**, (2017).

[18] A.S. Mischenko, Q. Zhang, R.W. Whatmore, J.F. Scott, and N.D. Mathur, Appl. Phys. Lett. **89**, 242912 (2006).

[19] A.S. Mischenko, Q. Zhang, J.F. Scott, R.W. Whatmore, and N.D. Mathur, Science (80-.). **311**, 1270 (2006).

[20] T.M. Correia, J.S. Young, and R.W. Whatmore, Appl. Phys. Lett **95**, 182904 (2009).

[21] O.M. Stafsudd and M.Y. Pines, J. Opt. Soc. Am. **62**, 1153 (1972).

[22] N.M. Shorrocks, R.W. Whatmore, and P.C. Osbond, Ferroelectrics **106**, 387 (1990).

[23] K.K. Deb, Mater. Lett. **5**, 222 (1987).

[24] R. Watton and M.A. Todd, Ferroelectrics **118**, 279 (1991).

[25] N.M. Shorrocks, S.G. Porter, R.W. Whatmore, A.D. Parsons, J.N. Gooding, and D.J. Pedder, Proc. SPIE 1320, Infrared Technol. Appl. **1320**, 88 (1990).

[26] N.W. Schubring, J. V. Mantese, A.L. Micheli, A.B. Catalan, and R.J. Lopez, Phys. Rev. Lett. **68**, 1778 (1992).

[27] J. Karthik and L.W. Martin, Appl. Phys. Lett. **99**, 032904 (2011).

[28] J. Karthik, J.C. Agar, A.R. Damodaran, and L.W. Martin, Phys. Rev. Lett. **109**, 257602 (2012).

[29] S. Pandya, G.A. Velarde, R. Gao, A.S. Everhardt, J.D. Wilbur, R. Xu, J.T. Maher, J.C. Agar, C. Dames, and L.W. Martin, Adv. Mater. **31**, 1 (2019).

[30] W.L. Warren, B.A. Tuttle, D. Dimos, G.E. Pike, H.N. Al-Shareef, R. Ramesh, and J.T. Evans,

Japanese J. Appl. Physics, Part 1 Regul. Pap. Short Notes Rev. Pap. **35**, 1521 (1996).

[31] J. Karthik, R.V.K. Mangalam, J.C. Agar, and L.W. Martin, Phys. Rev. B - Condens. Matter Mater. Phys. **87**, 1 (2013).

[32] Y. Zhou, H.K. Chan, C.H. Lam, and F.G. Shin, J. Appl. Phys. **98**, 0 (2005).

[33] J. Lee, R. Ramesh, V.G. Keramidas, W.L. Warren, G.E. Pike, and J.T. Evans, Appl. Phys. Lett. **66**, 1337 (1998).

[34] R.R. Mehta, B.D. Silverman, and J.T. Jacobs, J. Appl. Phys. **44**, 3379 (1973).

[35] R. Bruchhaus, D. Pitzer, M. Schreiter, and W. Wersing, J. Electroceramics **3**, 151 (1999).

[36] A. Berenov, P. Petrov, B. Moffat, J. Phair, L. Allers, and R.W. Whatmore, APL Mater. **9**, 041108 (2021).

[37] S. Pandya, G. Velarde, L. Zhang, and L.W. Martin, Phys. Rev. Mater. **2**, 1 (2018).

[38] Y. Liu, J.F. Scott, and B. Dkhil, Appl. Phys. Rev. **3**, 031102 (2016).

[39] S. Kar-Narayan and N.D. Mathur, J. Phys. D Appl. Phys **43**, 032002 (2010).

[40] S.G. Lu, B. Rožič, and Q.M. Zhang, Appl. Phys. Lett **97**, 162904 (2010).

[41] A.G. Chynoweth, J. Appl. Phys. **27**, 78 (1956).

[42] A.S. Mischenko, Q. Zhang, J.F. Scott, R.W. Whatmore, and N.D. Mathur, Science (80-.). **311**, 1270 (2006).

[43] B. Neese, B. Chu, S.G. Lu, Y. Wang, E. Furman, and Q.M. Zhang, Science (80-.). **321**, 821 (2008).

[44] B. Lu, P. Li, Z. Tang, Y. Yao, X. Gao, W. Kleemann, and S.G. Lu, Sci. Rep. **7**, 1 (2017).

[45] S. Crossley, R.W. Whatmore, N.D. Mathur, and X. Moya, APL Mater. **9**, 010701 (2021).

[46] X. Chen, S. Li, X. Jian, Y. Hambal, S.G. Lu, V. V. Shvartsman, D.C. Lupascu, and Q.M. Zhang, Appl. Phys. Lett. **118**, 122904 (2021).

[47] J. Lyu, I. Fina, R. Solanas, J. Fontcuberta, and F. Sánchez, Sci. Rep. **8**, 1 (2018).

[48] S. Jesse, A.P. Baddorf, and S. V. Kalinin, Appl. Phys. Lett. **88**, 062908 (2006).

[49] H. Qiao, O. Kwon, and Y. Kim, Appl. Phys. Lett **116**, 172901 (2020).

[50] M. Kawai, D. Kan, S. Isojima, H. Kurata, S. Isoda, Y. Shimakawa, S. Kimura, and O. Sakata, J. Appl. Phys. **102**, 114311 (2007).

[51] A.R. Damodaran, E. Breckenfeld, Z. Chen, S. Lee, and L.W. Martin, Adv. Mater. **26**, 6341 (2014).

[52] D.A. Tenne, X.X. Xi, Y.L. Li, L.Q. Chen, A. Soukiassian, M.H. Zhu, A.R. James, J. Lettieri, D.G. Schlom, W. Tian, and X.Q. Pan, Phys. Rev. B **69**, 174101 (2004).

[53] S. Kumar, D. Kumar, V.G. Sathe, R. Kumar, and T.K. Sharma, J. Appl. Phys. **117**, 134103

(2015).

[54] F. Liu, I. Fina, R. Bertacco, and J. Fontcuberta, Sci. Rep. **6**, 1 (2016).

[55] A. Picinin, M.H. Lente, J.A. Eiras, and J.P. Rino, Phys. Rev. B **69**, 064117 (2004).

[56] M. Vopsaroiu, J. Blackburn, M.G. Cain, and P.M. Weaver, Phys. Rev. B **82**, 024109 (2010).

[57] S.B. Lang, Phys. Today **58**, 31 (2005).

[58] S.B. Lang, L.H. Rice, and S.A. Shaw, J. Appl. Phys. **40**, 4335 (1969).

[59] Y. Matsushita, A. Nochida, T. Yoshimura, and N. Fujimura, Jpn. J. Appl. Phys. **55**, 10TB04 (2016).

[60] A. Gruverman and M. Tanaka, J. Appl. Phys. **89**, 1836 (2001).

[61] Y. Liu, X. Lou, M. Bibes, and B. Dkhil, Phys. Rev. B - Condens. Matter Mater. Phys. **88**, 1 (2013).

[62] V. V. Osipov, D.A. Kiselev, E.Y. Kaptelov, S. V. Senkevich, and I.P. Pronin, Phys. Solid State **57**, 1793 (2015).

[63] R.C. Miller and A. Savage, J. Appl. Phys. **32**, 714 (1961).

[64] Y. Bai, K. Ding, G.P. Zheng, S.Q. Shi, and L. Qiao, Phys. Status Solidi Appl. Mater. Sci. **209**, 941 (2012).

[65] X. Moya, E. Stern-Taulats, S. Crossley, D. González-Alonso, S. Kar-Narayan, A. Planes, L. Mañosa, and N.D. Mathur, Adv. Mater. **25**, 1360 (2013).

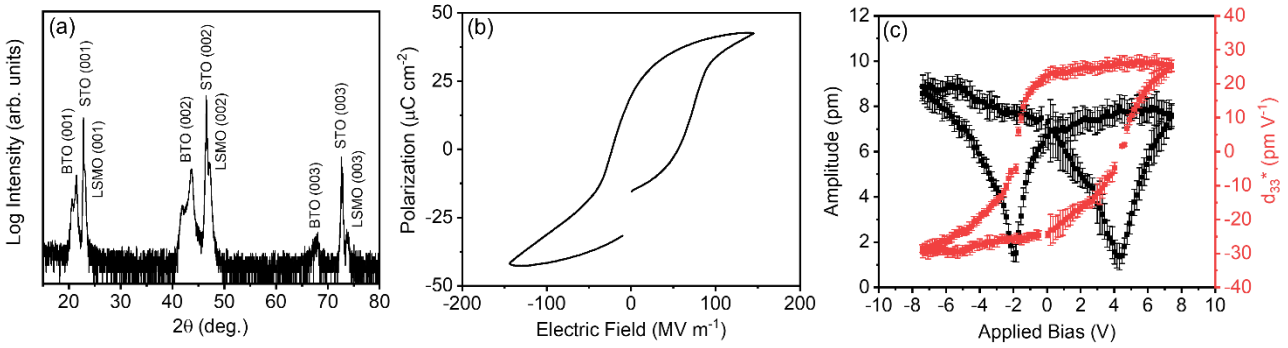

FIG. 1. (a) X-ray diffraction θ-2θ pattern of BTO/LSMO/STO(001). (b) P-E hysteresis loop, with ~ 16 MVm^{-1} positive imprint effect manifesting as a shift in the hysteresis loop to the right. (c) PFM hysteresis loop, which also exhibits a ~1 V imprint effect.

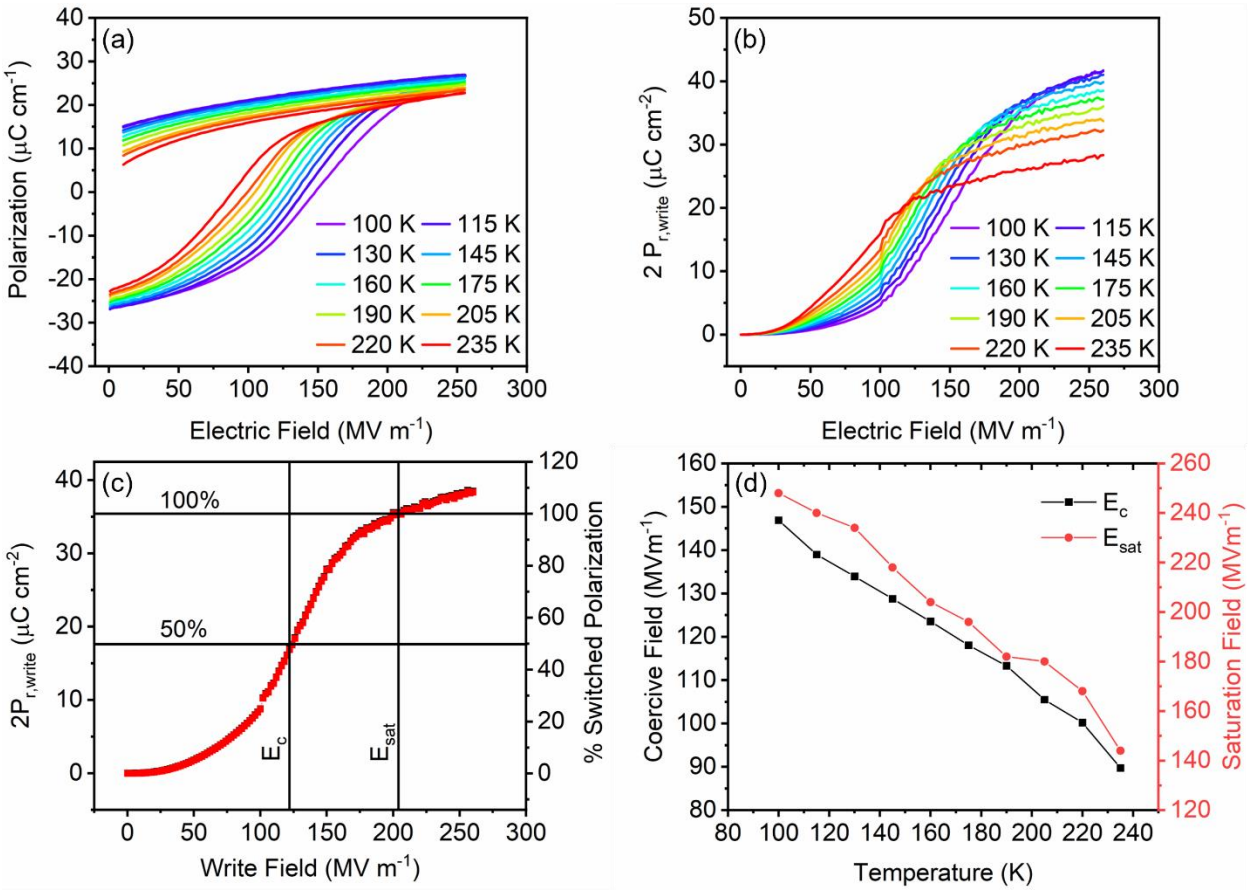

FIG. 2. (a) Second pulse (write) monopolar hysteresis loops collected from 100 K to 235 K, (b) evolution of the switchable polarization $2P_{r,write}$ with increasing second pulse field magnitude, (c) normalization of $2P_{r,write}$, and (d) evolution of coercive field E_c and saturation field E_{sat} with temperature.

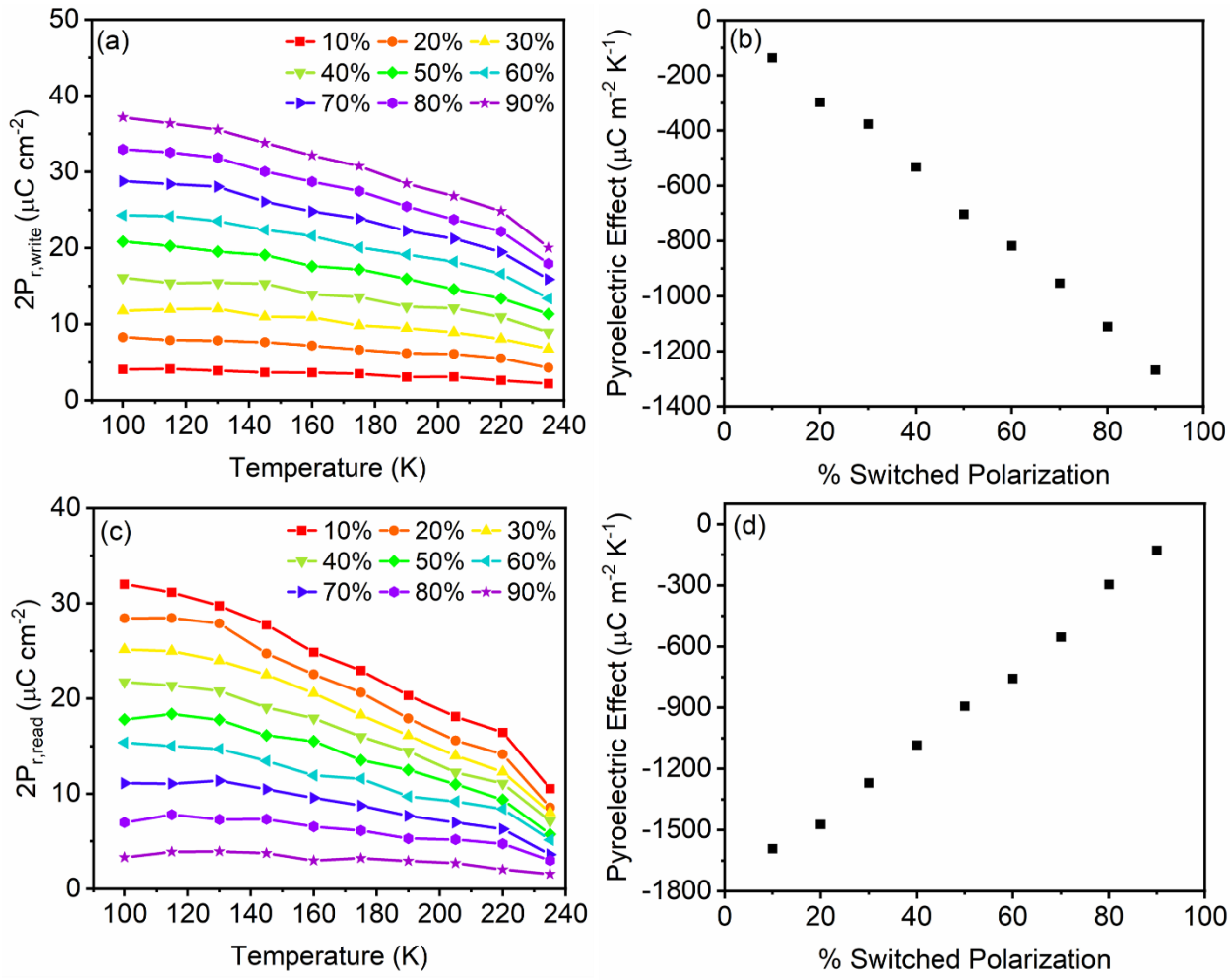

FIG. 3. Evolution of (a) $2P_{r,write}$ and (c) $2P_{r,read}$ from 100 K to 235 K at different polarization reversal extents. Evolution of pyroelectric effect calculated using (b) $2P_{r,write}$ and (d) $2P_{r,read}$ values at 100 K and 235 K versus polarization reversal.

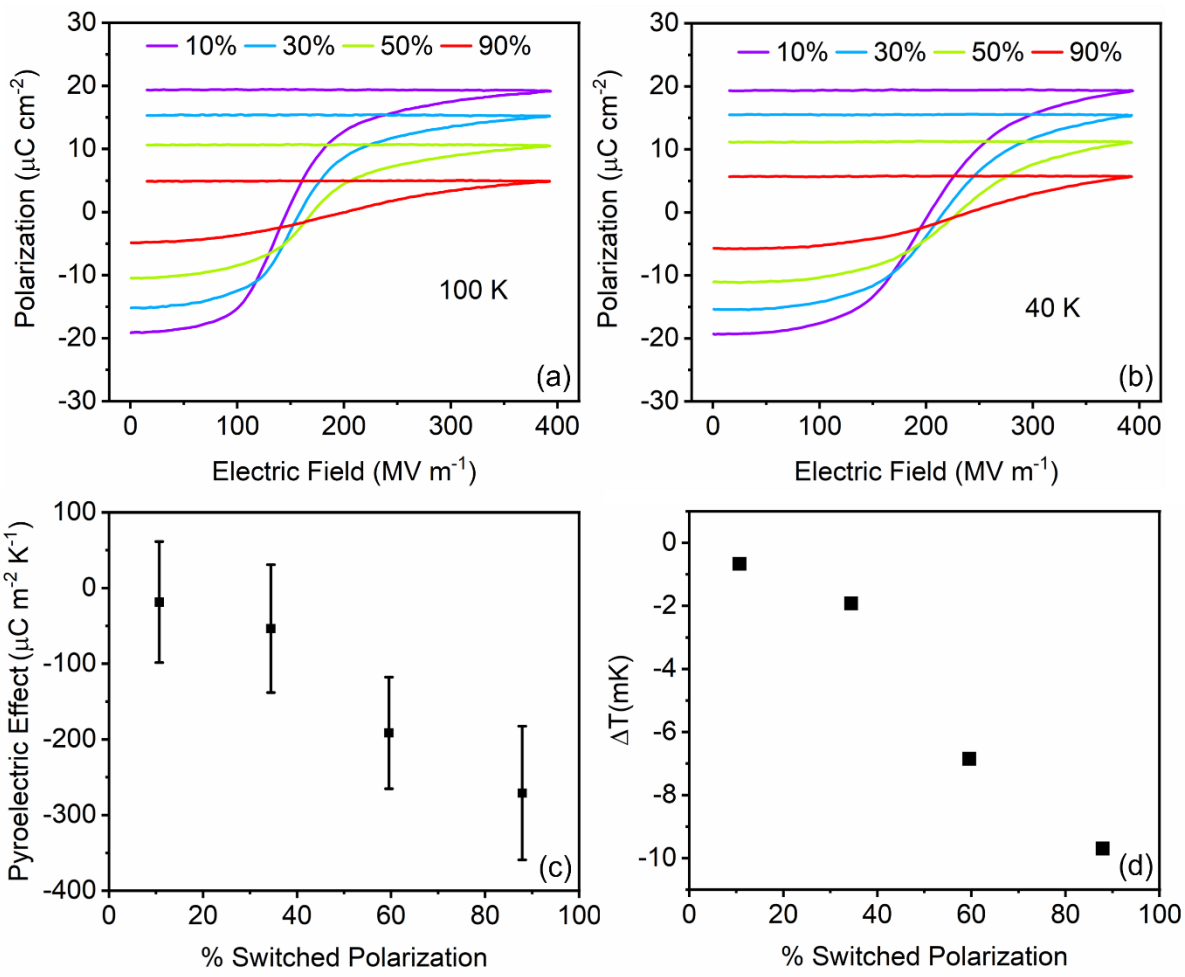

FIG. 4. Four-pulse protocol read loops collected at (a) 100 K and (b) 40 K for approximate polarization reversal extents. (c) Pyroelectric effect observed when taking difference in $2P_{r,read}$ for approximate polarization reversal extents. (d) Estimated temperature lift for approximate polarization reversal extents.